PTEP

Prog. Theor. Exp. Phys. **2019**, 113D02 (12 pages)
DOI: 10.1093/ptep/ptz120

Conceptual study on parasitic low-energy RI beam production with in-flight separator BigRIPS and the first stopping examination for high-energy RI beams in the parasitic gas cell

T. Sonoda[1,*], I. Katayama[1], M. Wada[2], H. Iimura[3], V. Sonnenschein[4], S. Iimura[1], A. Takamine[1], M. Rosenbusch[1], T. M. Kojima[1], D. S. Ahn[1], N. Fukuda[1], T. Kubo[1], S. Nishimura[1], Y. Shimizu[1], H. Suzuki[1], H. Takeda[1], M. Tanigaki[5], H. Tomita[4], K. Yoshida[1], and H. Ishiyama[1]

[1]*RIKEN Nishina Center for Accelerator-Based Science, 2-1 Hirosawa, Wako, Saitama 351-0198, Japan*
[2]*Wako Nuclear Science Center (WNSC), High Energy Accelerator Research Organization (KEK), Tsukuba, Ibaraki 351-0198, Japan*
[3]*Japan Atomic Energy Agency (JAEA), 2-4 Shirakata, Tokai-mura, Ibaraki 319-1195, Japan*
[4]*Faculty of Engineering, Nagoya University, Nagoya, Aichi 464-8603, Japan*
[5]*Institute for Integrated Radiation and Nuclear Science (KURNS), Kyoto University, Kumatori, Osaka 590-0494, Japan*
[*]E-mail: tetsu@riken.jp

Received August 22, 2019; Revised September 24, 2019; Accepted September 24, 2019; Published November 28, 2019

An in-flight separator performs the important role of separating a single specific radioactive isotope (RI) beam from the thousands of RI beams produced by in-flight fission as well as projectile fragmentation. However, when looking at "separation" from a different viewpoint, more than 99% of simultaneously produced RI beams are just eliminated in the focal plane slits or elsewhere in the separator. In order to enhance the effective usability of the RIKEN in-flight separator BigRIPS, we have been developing an innovative method: parasitic laser ion source (PALIS), which implements parasitic low-energy RI beam production by saving eliminated RI beams during BigRIPS experiments. In this paper, we present the expected benefits and feasibility for the PALIS concept and the results of the first stopping examination for high-energy RI beams in the gas cell.

Subject Index D50

1. Introduction

At the RI Beam Factory (RIBF) [1] in the RIKEN Nishina Center, cascaded cyclotrons accelerate all heavy ions up to approximately 350 MeV/nucleon. Significant performance has been achieved so far, such as a maximum beam current of 486 particle-nanoampere (pnA) for ^{78}Kr and 58 pnA for ^{238}U, respectively [2]. The superconducting in-flight separator BigRIPS [3] is a major device that produces high-energy RI beams (>200 MeV/nucleon) based on an in-flight separation technique for research with exotic nuclei. However, beam time at the RIBF is often limited due to expensive operational costs, while there are still many unknown physical properties for exotic nuclei such as electromagnetic moments, spin and mass that are of importance in nuclear physics. For those

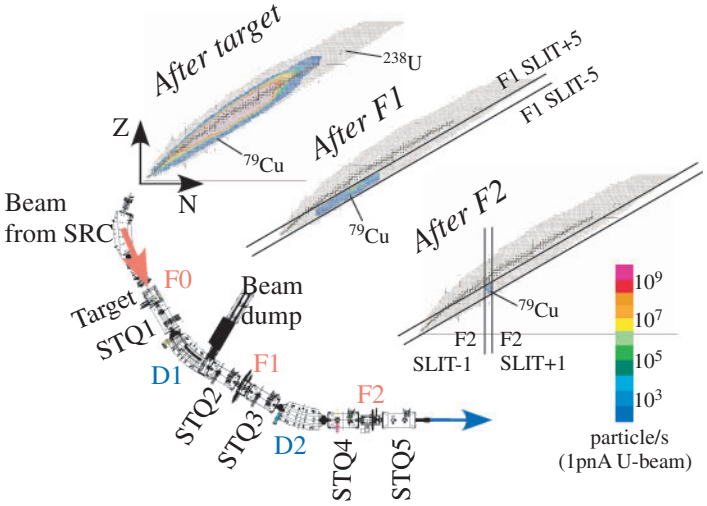

Fig. 1. The first stage of BigRIPS. The beam separation process in the case of in-flight fission for ^{79}Cu is visually shown by coloring the RIs in three nuclear charts, calculated by LISE^{++}. The left chart shows the RIs arriving at D1, and the central chart is the RI group after the F1 slits are horizontally set to ± 5 mm. The right chart is the RI group after the F2 slits are horizontally set to ± 1 mm.

comprehensive measurements, considerable time and expense would be required, even though new-generation RI beam facilities are in operation all over the world.

Here, we focus on two facts. (1) The opportunity to produce and investigate rare isotopes is not easily obtained. (2) The in-flight separator BigRIPS has a great capability to produce rare isotope beams, but only a few rare isotope beams are used in one experiment, while thousands of simultaneously produced isotope beams are discarded. In view of these facts, we propose the idea of saving unused RI beams by parasitic low-energy RI beam production (parasitic laser ion source, PALIS) [4,5] coupled to BigRIPS to establish effective utilization of rare isotopes and to perform comprehensive measurements of physical properties of exotic nuclei.

In the PALIS system, relativistic RI beams produced by BigRIPS are decelerated and cooled in a gas cell, and the extracted low-energy RI beams are utilized for a wide range of precision atomic and nuclear spectroscopy. PALIS consists of several functional devices, such as a beam extraction and pumping system [6], a gas circulation and purification system [7], and a laser optical system [8,9]. These devices have been successfully constructed at the second focal plane (F2) at BigRIPS and the whole system is currently in the commissioning stage. In the future, the extracted RI beam from PALIS will be sent to the detector station for low-energy RI experiments via the SLOWRI beam line [10].

In this paper, we discuss the expected benefits and feasibility of PALIS using realistic situations in past BigRIPS experiments. Also, the results of an on-line experiment for the stopping examination of a high-energy RI beam are presented.

2. Expected benefits of the PALIS concept

The in-flight separator BigRIPS has many outstanding features such as a large ion-optical acceptance, a two-stage structure, and excellent particle identification. The angular acceptance is ± 40 mrad horizontally, ± 50 mrad vertically, and the momentum acceptance is $\pm 3\%$. This allows approximately 50% efficiency for the collection of fission fragments in the case of in-flight fission. Figure 1 shows

the first stage of BigRIPS, which consists of two dipoles (D1 and D2) and four superconducting triplet quadrupoles (STQ1–STQ4) located between the production target F0 and the achromatic focus F2. This configuration forms a two-bend achromatic system with the momentum-dispersive focus at F1. Owing to a technique called the momentum-loss achromat [11], RI fragments are isotopically separated in flight by a combination of magnetic analysis and energy loss. The energy loss arises at the dispersive focus at F1 using a wedge-shaped achromatic energy degrader.

In this separation stage, the region around the RI of interest is roughly cut off from vast amounts of a variety of RIs produced in the target via selection of the mass-to-charge ratio A/Z by the parameter Bρ at D1. This causes many unused RI beams to hit the beam dump in the D1 and F1 slits, while specific isotone chains including the RI of interest arrive at F2. The F2 slits then eliminate those isotone chains near the RI of interest, producing a high-purity RI beam in the first stage. The upper half of Fig. 1 shows colored RI beams in three nuclear charts calculated by LISE^{++} [12,13], which reveal the beam separation process in the case of in-flight fission for ^{79}Cu. A variety of RIs except those in the vicinity of the RI of interest are thus eliminated in the first stage of BigRIPS.

In terms of the eliminated RI beam collection at PALIS, locations at D1 and before the F1 slits in BigRIPS are the most ideal to collect a large number of unused RI beams. However, very high-level radiation near the beam dump may hinder the development of new components. Therefore, we have decided to install PALIS at F2 as the first step. As described above, only limited isotone chains neighboring the RI of interest arrive at F2. However, various RI beams are still available, including many rare isotopes. Experimental users typically request rare isotopes near the limits of production capability, so that the neighbors of the requested RI beam also include very rare isotopes.

Figures 2 and 3 show examples of RI beams and their yields arriving at F2 in the assumed BigRIPS experiments, calculated by LISE^{++}. In the first example shown in Fig. 2, a ^{67}Se beam is produced by projectile fragmentation with the primary beam ^{78}Kr. Experimental users often request that the horizontal F1 slits stay as closed as possible for beam purification. However, when they are severely closed, the yield of the ^{67}Se beam decreases, depending on its beam size (energy spread). Therefore, the status of the F1 slits depends on the experimental aim. If the priority is to maximize the yield, then the slits should be opened to the same size as that of the beam. The LISE^{++}-calculation in Fig. 2 had a yield priority, and the horizontal F1 slits were set to $\pm$5 mm in the calculation. Among the RIs eliminated at the F2 slits, the yield of, e.g., ^{57}Cu was estimated to be 3×10^3 particles/second (pps) with 300 pnA of the primary ^{78}Kr beam. This would be sufficient for a nuclear physics experiment, such as in-gas cell laser spectroscopy [14,15]. In the second example, Fig. 3 shows the situation for in-flight fission of a ^{238}U beam for a ^{126}Sn beam. Many neutron-rich RI beams appear at F2 to the left and right sides of the central ^{126}Sn beam, when the horizontal F1 slits are set to $\pm$5 mm. For example, the yield of double-Magic ^{132}Sn, which will hit the F2 slit, can be at the 10^5 pps level, when the primary beam of ^{238}U is 20 pnA. Particle yields of that order are attractive for many kinds of nuclear physics experiments.

These realistic estimates indicate that even though a majority of RI beams produced at the target are swept up at the beam dump in D1 and the F1 slits, there are still many rare isotope beams available for PALIS at F2. Furthermore, those unused RI beams are available at no extra cost, whenever the BigRIPS experiments are in operation.

3. Requirement and feasibility for PALIS

To establish PALIS, it is necessary to collect unused isotope beams before they are dumped at slits. Also, the gas cell should be able to move along the horizontal (x) axis perpendicular to the main

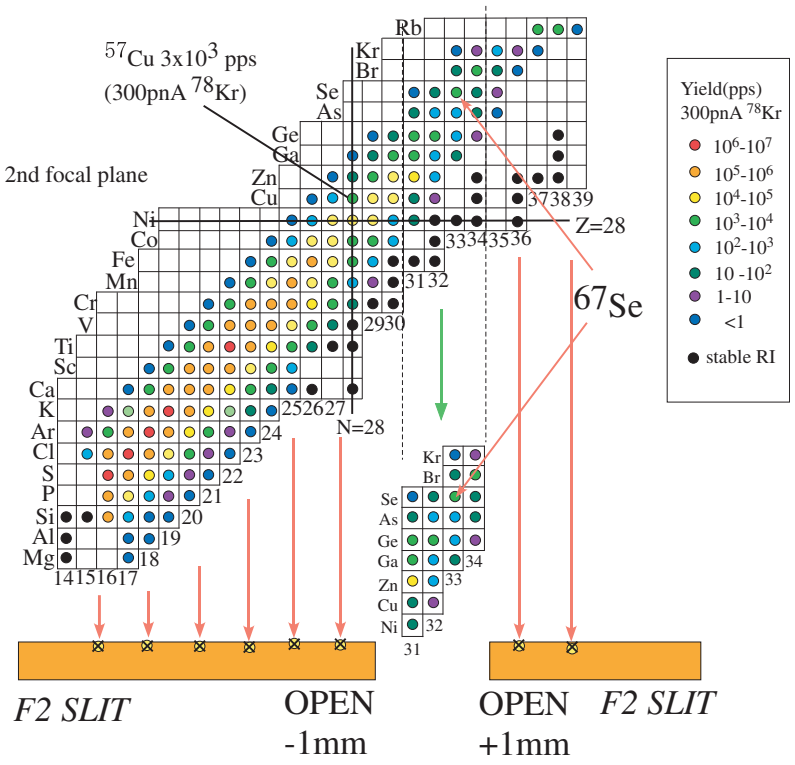

Fig. 2. As a first example of the BigRIPS experiments, RI beams (different colored circles for different yields) arriving at the F2 are shown in part of a nuclear chart, calculated by LISE^{++}. The RI of interest here is ^{67}Se, produced by ^{78}Kr + Be projectile fragmentation. Partial RI beams including ^{67}Se pass through the F2 slits ($\pm$1 mm horizontally), while many unused RI beams are discarded at the F2 slits. The horizontal F1 slits are set to $\pm$5 mm.

beam to collect various unused RI beams. Importantly, there should be no interference with the main BigRIPS experiment. As shown in Fig. 4, a combined energy degrader and small gas cell is placed in front of the F2 slits and can move along the x-axis. To avoid interference with the central RI beam, the beam width should be considered when the gas cell is moved. Figure 5 shows a schematic of the F2 slits with the gas cell and the central beam (left), and it also shows an example of a LISE^{++} result simulating the central beam profile on horizontal space at the front plane of the gas cell (right). This example is a fission fragment ^{79}Se beam produced in the ^{238}U + Be reaction with 6 mm of an aluminum achromatic energy degrader used at F1. The horizontal F1 slits are fully open. The distance in the direction of the beam axis between the F2 focal plane and the front plane of the gas cell is 46 cm. At the front plane of the gas cell, the beam shape is broadened due to the position before final focusing. The horizontal full-beam width is $\Delta X = 30.0$ mm; thus the gas cell edge can be $> +15$ mm or < -15 mm from the central beam along the x-axis.

Interference of the central beam transmission by varying the gas cell position was experimentally investigated with the BigRIPS beam. The central beam was ^{79}Se with 200 MeV/nucleon and the yield was counted with the downstream plastic scintillator located in the third focal plane chamber (F3) in BigRIPS. There was no interruption of the central beam passage, unless the gas cell came within $\pm$ 15 mm of the central beam axis. This was consistent with the simulation in Fig. 5.

To choose the unused isotope beams in PALIS, the gas cell should be moved to the appropriate position on the x-axis, depending on the RI of interest for the PALIS user. Figure 6 shows an example

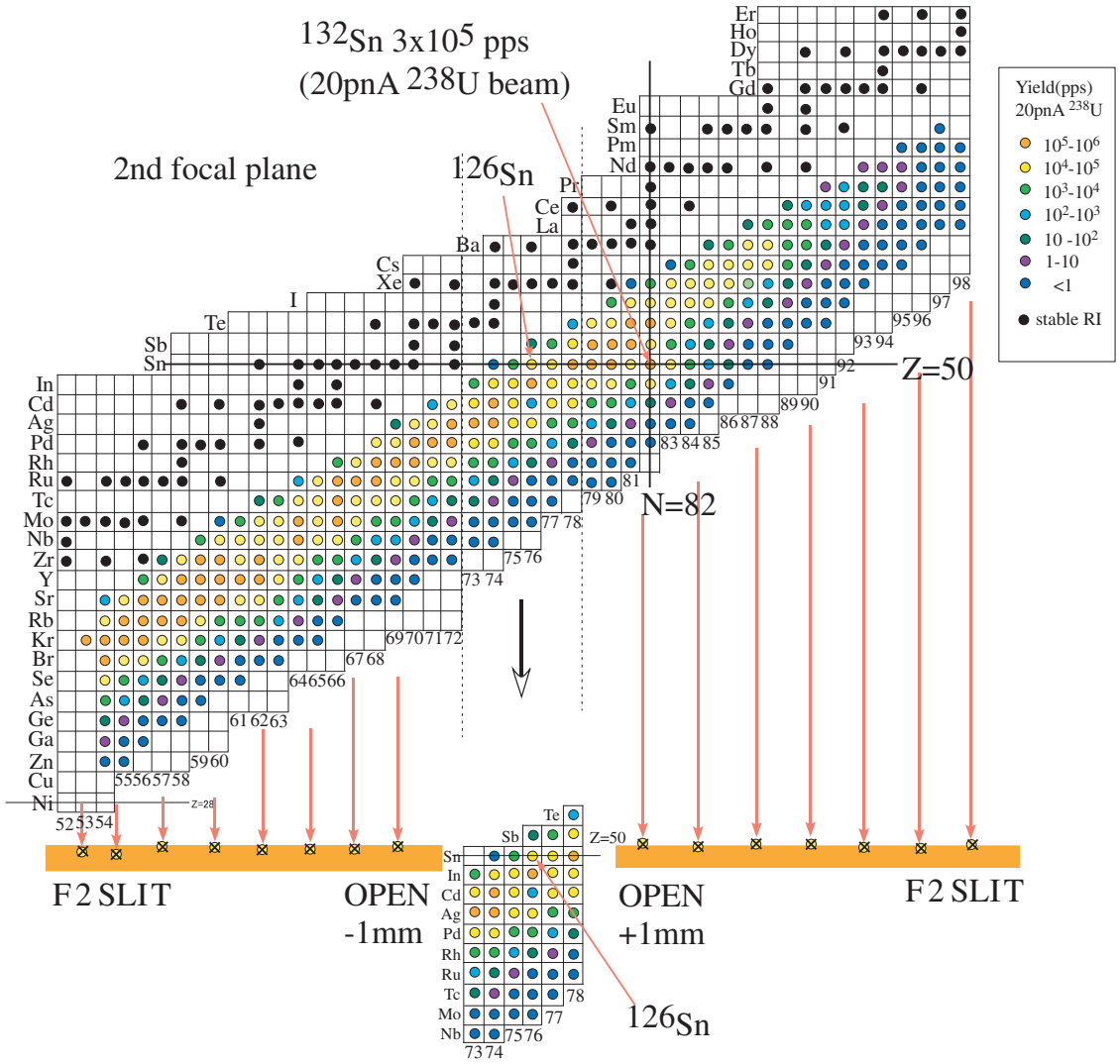

Fig. 3. As a second example of the BigRIPS experiments, RI beams (different colored circles for different yields) arriving at F2 are shown in part of a nuclear chart, calculated by LISE^{++}. The RI of interest here is ^{126}Sn, produced by ^{238}U + Be in-flight fission. Except for the RI beams close to ^{126}Sn, many neutron-rich RI beams hit the F2 slits. The central RI beams passing through F2 when the slits are closed to ± 1 mm in the horizontal axis are also shown. The horizontal F1 slits are set to ± 5 mm.

of LISE^{++} results for the Se isotope distribution along the horizontal axis at the F2 focal plane under the same conditions as in Fig. 5. Thus, unused isotope beams with a central ^{79}Se beam arrive at the right and left sides, symmetrically distributed with respect to the central beam. The distance between each isotope along the x-axis was about 6 mm. In PALIS, we can select the RI of interest by moving the gas cell without interrupting the central beam. However, if the gas cell has to cross the central beam, it should be done during beam-off periods.

Considering the practical feasibility of PALIS, it is a parasitic experiment within a main BigRIPS experiment, and all control parameters related to BigRIPS and the authority of the beam ON/OFF are dependent on the main users. Understandably, the magnetic rigidity (Bρ) of D1 and D2 in BigRIPS cannot be changed by the PALIS user. In nuclear measurements such as decay spectroscopy and laser spectroscopy, continuous time under constant conditions is often necessary for sufficient statistics. Therefore, if Bρ is changed frequently by the main user, it is difficult to perform PALIS experiments.

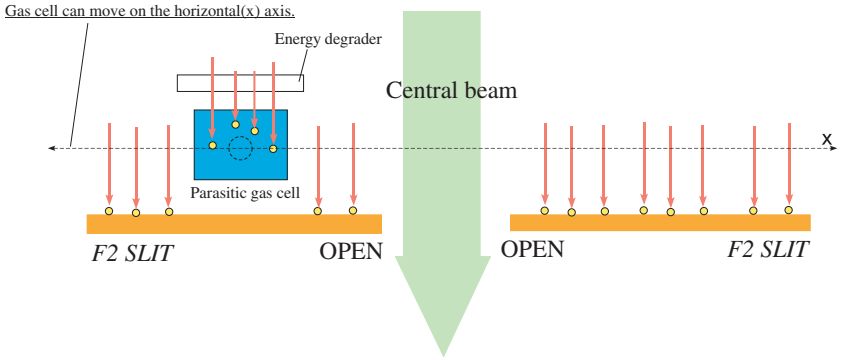

Fig. 4. Schematic view of PALIS at F2 in BigRIPS. Unused RI beams enter the gas cell through an energy degrader, before they hit the slits. These saved RIs are thermalized in the gas cell and extracted for low-energy RI experiments.

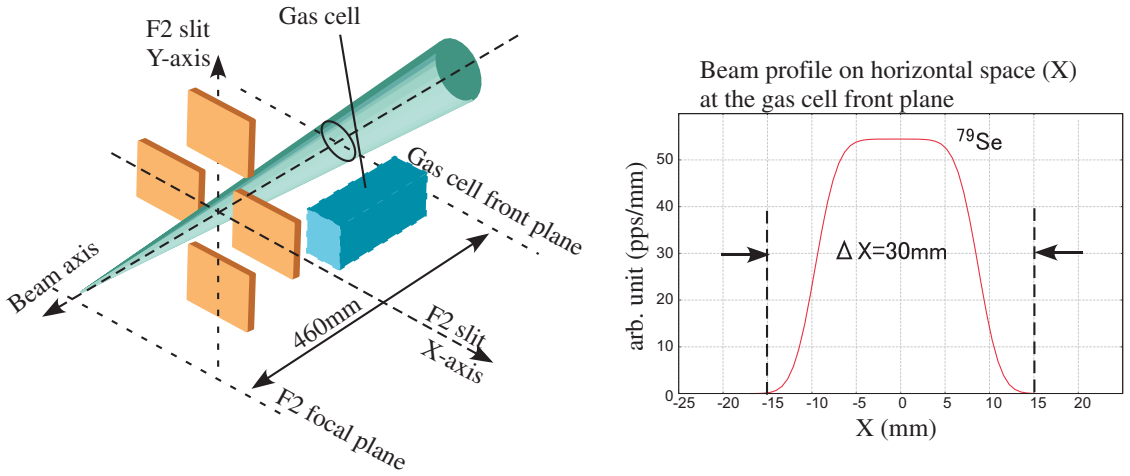

Fig. 5. Left: A schematic of the F2 slits and the PALIS gas cell. The beam is gradually focused at the focal plane. Right: LISE^{++}-simulated horizontal beam profile at the front plane of the gas cell, located 46 cm upstream of the focal plane in F2.

However, BigRIPS optical parameters, including Bρ, are normally not changed frequently. Figure 7 shows an example of a time chart for the magnetic rigidity at D1 and D2 in an actual BigRIPS experiment. Both Bρ stayed constant for up to a week. A typical BigRIPS experimental procedure is as follows: (1) BigRIPS operators adjust the optical parameters for the requested RI beam, which takes a certain time (often 12 hours or more). (2) BigRIPS operators serve the RI beam to the user, who then starts measurements. By following this procedure, the PALIS experiment will have a sufficient time during main user measurements.

We are finalizing the extraction of thermalized and stopped RI beams in gas, and plan to apply two different schemes. The first (A) is based on laser ionization in the gas [16], the second (B) is based on the IGISOL (ion guide isotope separator on-line) technique [17]. A major difference between these two techniques is the type of gas: (A) uses argon, while (B) uses helium. In both, the RI motion towards the gas cell exit is attributed to gas flow. In (A), the energy-reduced RI-ions are thermalized in the argon gas and eventually neutralized. The neutralized RIs are then photo-ionized by a laser. High-purity low-energy RI beams can be produced via element-selective resonant ionization [18]. In (B), we utilize the nature of helium such that some of the thermalized ions are retained as singly or doubly

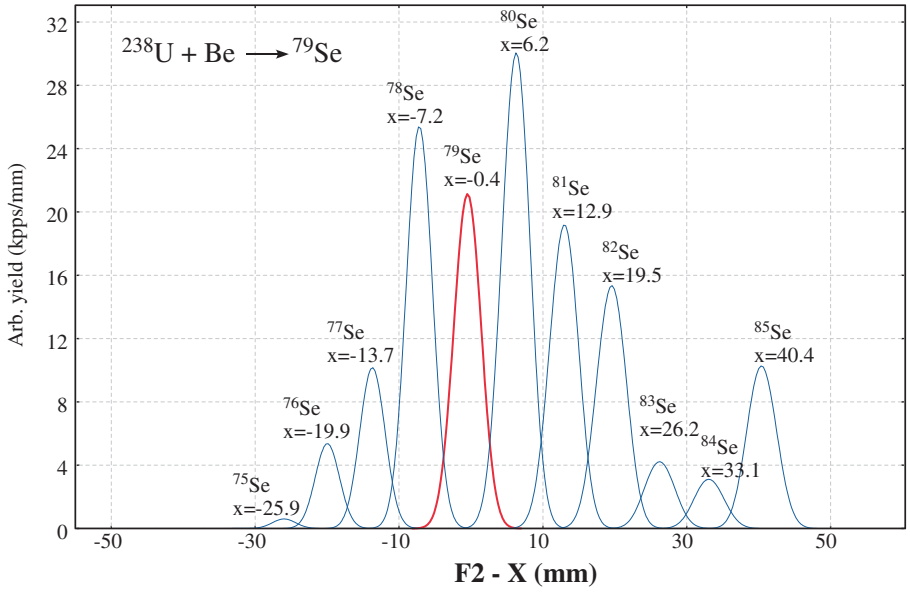

Fig. 6. Selenium isotope distribution along the horizontal axis at the F2 focal plane, simulated by LISE^{++}. The central beam is ^{79}Se produced in ^{238}U + Be in-flight fission. The F1 slits are fully open.

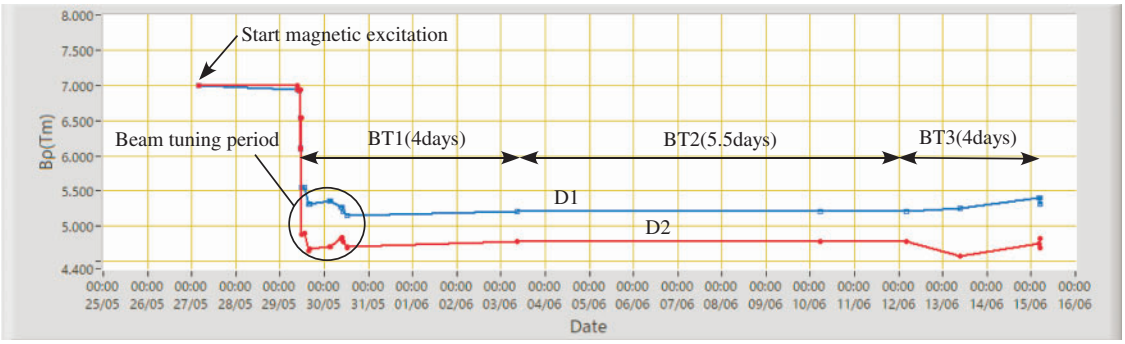

Fig. 7. A sample time chart for the magnetic rigidity at D1 and D2 in a BigRIPS experiment. There were three different beam times (BT) over 25 May–16 June 2019.

charged ions, which are extracted by gas flow. Both schemes have advantages and disadvantages. Argon has a stopping power that is ten times that for helium, whereas the extraction time in helium is three times faster than that in argon. Although argon gas flow is relatively slow, which causes a loss by decay of short-lived nuclei, it is still suitable for RIs with half-lives above 50 milliseconds. As a spin-off of (A), it is also possible to perform laser spectroscopy. During resonant ionization, hyperfine splittings and isotope shifts can be measured to determine nuclear spins, moments, and charge radii. Novel spectroscopy experiments such as in-gas-cell [14,15] and in-gas-jet laser spectroscopy [19–22] will be performed in future PALIS experiments.

Table 1 shows the expected individual efficiency for the overall efficiency of the extraction schemes (A) and (B). We assume that the RI has a half-life $T_{1/2}$ of 0.5 s and an impurity level in the gas of 1 ppb with 1×10^{-10} cm^3/s of rate constant for the formation of an ion-molecular or an atom-molecular. In this condition, we expect the overall efficiency of PALIS to be 4.8% for (A) and 0.3% for (B). There is a difference between (A) and (B), mainly caused by the stopping efficiency. These efficiencies were evaluated by referring to the simulation and the past experimental records obtained at LISOL

Table 1. Expected individual efficiency for the overall efficiency of the extraction schemes (A) and (B) (e.g., RI($T_{1/2} = 0.5$ s)).

Expected individual efficiency	Extraction scheme (A)	Extraction scheme (B)
Stopping efficiency	30%	3%
Neutralization/survival of ions	99%	30%
Survivability against diffusion	76%	45%
Survivability against molecular formation	48%	87%
Survivability against decay loss	55%	91%
Laser ionization + spatial overlapping	100%	—
Ion transmission to the high vacuum	80%	80%
Overall efficiency	4.8%	0.3%

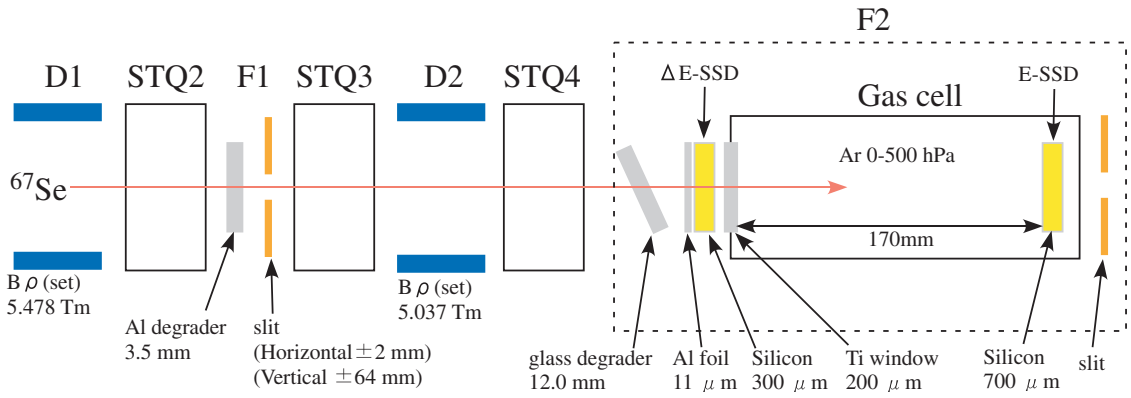

Fig. 8. Schematic of the experimental setup from D1 to F2 in BigRIPS.

[16] and IGISOL [17], except for the stopping efficiency. Realistically, the individual efficiencies depend on the gas cell dimensions, the type of element of extracted RI, the laser condition, the type of impurity, the implanted beam condition, etc.

4. First stopping examination for high-energy RI beam in PALIS

In a PALIS experiment, the energy difference from the initial (>300 MeV/nucleon) to the final stopping condition (<1 eV in total kinetic energy) spans over nine orders of magnitude. Therefore, we confirmed the reliability of the stopping calculation with on-line radioactive beams. A schematic of the experimental setup from D1 to F2 in BigRIPS is shown in Fig. 8. This experiment used the central RI beam; the gas cell was therefore located at the central beam axis. Two silicon surface barrier detectors (SSD) were installed inside the F2 chamber and used for examining the ΔE–E relation. The first detector (ΔE-SSD) was mounted just after the glass energy degrader and the second one (E-SSD) was mounted inside the gas cell. A ^{78}Kr primary beam was delivered from the RIBF cascaded cyclotrons with an energy of 345 MeV/nucleon. The primary beam impacted a 2.0-mm-thick beryllium target, producing fragmentation products. The beam line was tuned to optimize the radioactive ^{67}Se beam by adjusting the BigRIPS optical parameters. At F1, the RI beams, roughly separated by the D1 rigidity set for ^{67}Se, passed through a 3.5-mm-thick aluminum wedge degrader at an angle of 4.2 mrad and passed through the slits set to ±2 mm horizontally and ±64 mm vertically. The radioactive beams after the F1 slit were composed of several isotone chains including the ^{67}Se beam. After STQ4, the high-energy beams were sent through a borosilicate glass (BSL7) degrader

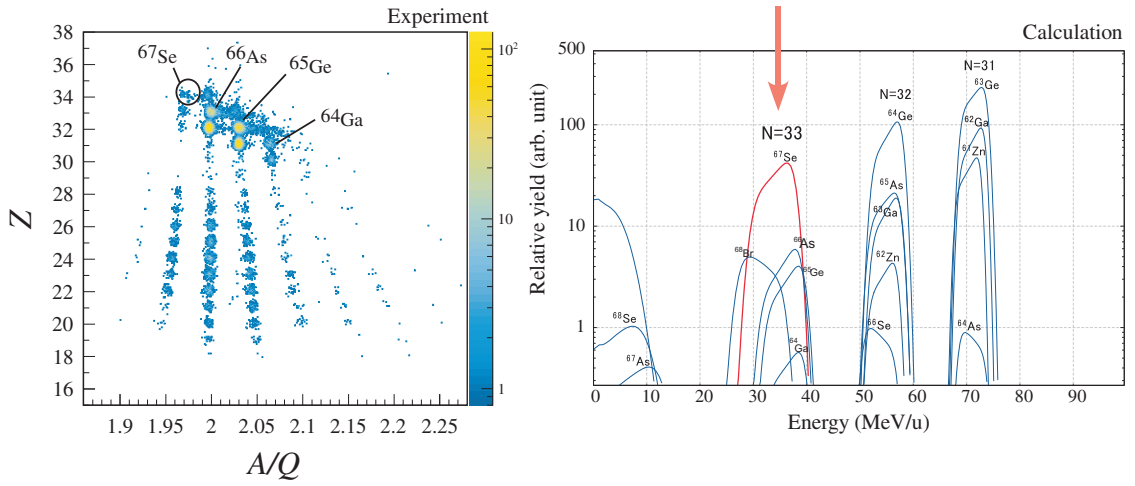

Fig. 9. Left: Experimental data on Z vs. A/Q plot optimized for ^{67}Se projectile fragments produced in the ^{78}Kr + Be reaction at 345 MeV/nucleon. Right: Energy distribution after the 13.46-mm-thick glass degrader calculated by LISE^{++}.

with a thickness range of 12.0–13.9 mm that was rotationally adjusted by a stepping motor with a minimum angular step of 0.25 degrees. In Fig. 9, the left panel shows the particle identification plot measured by the BigRIPS regular detectors. We confirmed clear peaks from fully stripped ^{67}Se, ^{66}As, ^{65}Ge, ^{64}Ge, ^{64}Ga, and ^{63}Ga. The right panel shows the calculated energy distribution after the glass energy degrader when its thickness was 13.46 mm (27 degrees). Each isotone beam with the same neutron number $(N) = 31, 32, 33$ was well separated energetically. Here, the $N = 33$ isotone beam, consisting of ^{67}Se, ^{66}As, ^{65}Ge, and ^{64}Ga, was adjusted to maximize the stopping efficiency in the gas.

After the glass degrader, there were three components that reduced the beam energy before it entered the argon gas. The first was an 11-μm-thick aluminum foil upstream that covered ΔE-SSD. The second was a 300-μm-thick ΔE-SSD with an active area of 300 mm^2. The last was a 17-mm-thick titanium window with a diameter of 200 μm, which separated the argon gas cell from the vacuum. After the titanium window, the beam passed through the argon to the E-SSD where the gas volume was $40\phi \times 170$ mm. Finally, the beam terminated at E-SSD or the metallic assembly fixed on the backside of E-SSD. The active area and thickness of the E-SSD were 150 mm^2 and 700 μm, respectively. Energy loss spectra were obtained with ΔE-SSD and E-SSD, as the angle of the glass degrader was varied from 18 to 28 degrees. Due to a lack of beam time, angle steps were restricted to every one or two degrees. To protect the detector, the total radioactive beam intensity entering ΔE-SSD was carefully adjusted to be several hundred particles per second. Figure 10 shows ΔE–E energy loss scatterplots when the angle of the glass degrader was set to 18 (top plots) and 22 degrees (bottom plots) at a 440 mbar gas cell pressure. On the left is the Monte Carlo simulation in LISE^{++} and on the right are the experimental data.

In the LISE^{++} calculation, all parameters including the target and F1 degrader thicknesses and the density of all materials used for energy degradation were set as close as possible to the experimental values. However, the Bρ value at D1 had to be adjusted, because there was no precise monitor for magnetic field due to the high radiation in the D1 area. In the experiment, the set Bρ value for D1 was 5.4780 Tm, while the final adjusted Bρ value in LISE^{++} was 5.5000 Tm, when the experimental data agreed with the calculations. In Fig. 10, an ensemble of isotones ($N = 33$) consisting of ^{67}Se,

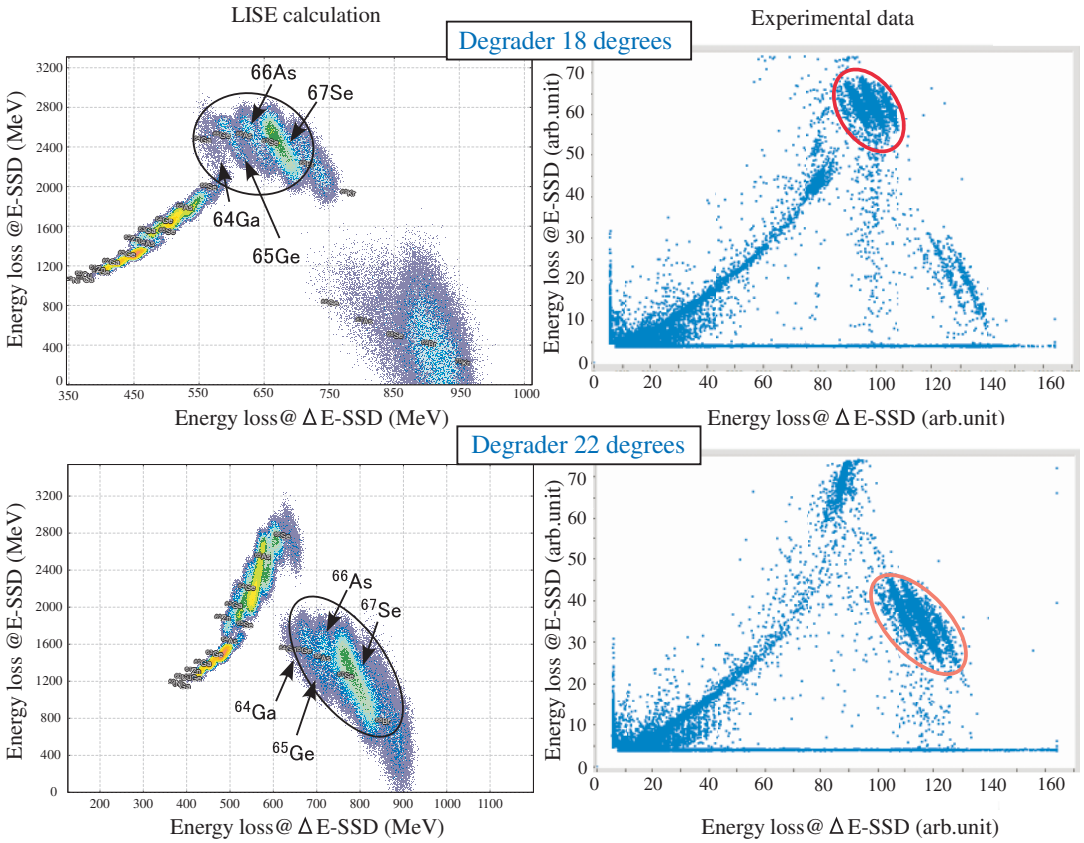

Fig. 10. E vs. ΔE plots for angles of the glass energy degrader of 18 degrees (top) and 22 degrees (bottom) with a 440 mbar gas cell pressure. Left: Monte Carlo simulation in LISE^{++}. Right: Experimental data taken with two silicon surface barrier detectors.

^{66}As, ^{65}Ge, ^{64}Ga appeared in both results. We confirmed that this ensemble moved together within the E–ΔE plot, when the degrader angle was varied. This was consistent in the calculations and experiments, as shown in Fig. 10.

To estimate the transmitted fraction at E-SSD, we integrated the total counts involving this ensemble at every degrader angle (total counts in the inner red circle in the right panels in Fig. 10). The total counts were normalized by the measurement time and the primary beam intensity. The normalized transmitted and expected stopped fractions as a function of the degrader angle for no gas (green rhombuses) and 440 mbar argon (red circles) in the gas cell are plotted in Fig. 11. The experimental data at 440 mbar were compared with those expected by the LISE^{++} calculations illustrated in Fig. 11 by blue squares and the dashed line. Good agreement can be achieved by a slight adjustment of Bρ at D1 in LISE^{++}, as mentioned above. In addition, the expected stopped fraction in the gas that was estimated in calculations is illustrated in Fig. 11 (white squares and solid line by LISE^{++}, purple circle from experimental data at 24 degrees). Approximately 30% of the ensemble of $N = 33$ isotone beams was stopped in 440 mbar argon at the optimum degrader angle. From the present on-line test, we confirmed several facts. (1) The geometries of the energy degrader, the gas cell, and the two silicon surface barrier detectors were correctly aligned with the BigRIPS beam axis. (2) The LISE^{++} calculation was reproducible in the experimental data, even if the energy range was beyond 300 MeV/nucleon. (3) At F2, an energetic separation of each isotone was available after the

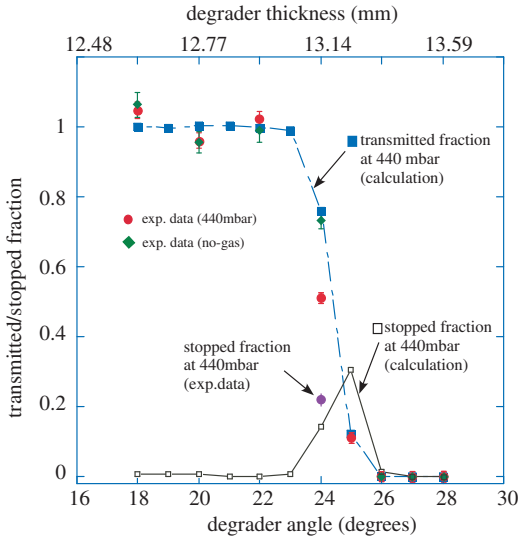

Fig. 11. Normalized transmitted and estimated stopped fractions as functions of the degrader angle at 440 mbar gas cell pressure. The degrader angle and its thickness are indicated on the top and bottom horizontal axes. The LISE^{++} calculation of the transmitted fraction is shown as a dashed line. The stopping fraction estimated from LISE^{++} is also shown (solid line).

energy degrader. It can help to optimize the stopped fraction of the RI of interest within the available isotopes in the PALIS experiment.

5. Summary

We have presented the expected benefits and feasibility of PALIS at F2 in BigRIPS. Simulations were based on realistic situations of BigRIPS experiments. For maximal saving of unused RI beams in BigRIPS, the beam dump region in D1 or the location in front of the F1 slits were the most ideal because of the high intensity and availability of various RI beams. However, many varieties of rare isotope beams are also ready for use at F2. Because of the parasitic nature of the experiment, frequent changes of Bρ at D1 or D2 by a main user would hinder applicability. However, the BigRIPS optical parameters typically remain constant for up to a week, according to past records, although this depends on the main experimental schedule. Currently we expect the overall efficiency of PALIS to be a maximum of about 5%, depending on the extraction scheme. The experimental measurement for overall efficiency is planned for the near future. The authors emphasize that PALIS doubles the usability of the RIBF experiment without extra operational costs. Ideally, the beam time can be used during all BigRIPS experiments, which currently corresponds to about five months a year.

We have provided on-line experimental results for stopping high-energy RI beams passing through various solid materials and gases. A clear confirmation was achieved that LISE^{++} calculations well reproduced the experimental results. We estimated a stopped fraction of approximately 30% at 440 mbar gas cell pressure, against a total number of $N = 33$ isotone beams.

As a next step, we will establish the extraction technique of stopped RIs for low-energy RI beams.

Acknowledgements

We wish to thank the RIKEN Nishina Center for Accelerator-Based Science for financial support of this research. This experiment was performed at the RI Beam Factory operated by RIKEN Nishina Center and

CNS, University of Tokyo. The authors would like to thank the accelerator crew at RIBF who provided high-quality beam. We are grateful to the BigRIPS team for their fruitful support and understanding during development.

References

[1] Y. Yano, Nucl. Instrum. Meth. B **261**, 1009 (2007).
[2] RIBF Technical Information web site - Beam intensity (Nov. 2019), available at: http://www.nishina.riken.jp/RIBF/accelerator/tecinfo.html.
[3] T. Kubo, Nucl. Instrum. Meth. B **204**, 97 (2003).
[4] T. Sonoda et al. [SLOWRI Collaboration], AIP Conf. Proc. **1104**, 132 (2009).
[5] T. Sonoda et al., Hyperfine Interact. **216**, 103 (2013).
[6] T. Sonoda et al., Nucl. Instrum. Meth. B **295**, 1 (2013).
[7] T. Sonoda, T. Tsubota, M. Wada, I. Katayama, T. M. Kojima, and M. Reponen, Rev. Sci. Instrum. **87**, 065104 (2016).
[8] T. Sonoda, H. Iimura, M. Reponen, M. Wada, I. Katayama, V. Sonnenschein, T. Takamatsu, H. Tomita, and T. M. Kojima, Nucl. Instrum. Meth. A **877**, 118 (2018).
[9] M. Reponen, V. Sonnenschein, T. Sonoda, H. Tomita, M. Oohashi, D. Matsui, and M. Wada, Nucl. Instrum. Meth. A **908**, 236 (2018).
[10] M. Wada et al., RIKEN Accel. Prog. Rep. **47**, 203 (2013).
[11] K.-H. Schmidt, E. Hanelt, H. Geissel, G. Münzenberg, and J. P. Dufour, Nucl. Instrum. Meth. A **260**, 287 (1987).
[12] O. B. Tarasov and D. Bazin, Nucl. Instrum. Meth. B **266**, 4657 (2008).
[13] O. B. Tarasov and D. Bazin, LISE++ (v.11.2,2019) web site, Michigan State University, available at: http://lise.nscl.msu.edu/lise.html.
[14] T. E. Cocolios et al., Phys. Rev. Lett. **103**, 102501 (2009).
[15] R. Ferrer et al., Phys. Lett. B **728**, 191 (2014).
[16] Y. Kudryavtsev et al., Nucl. Instrum. Meth. B **114**, 350 (1996).
[17] J. Äystö, Nucl. Phys. A **693**, 477 (2001).
[18] V. N. Fedosseev, Yu. Kudryavtsev, and V. I. Mishin, Phys. Scripta **85**, 058104 (2012).
[19] T. Sonoda, T. E. Cocolios, J. Gentens, M. Huyse, O. Ivanov, Yu. Kudryavtsev, D. Pauwels, P. Van den Bergh, and P. Van Duppen, Nucl. Instrum. Meth. B **267**, 2918 (2009).
[20] R. Ferrer et al., Nucl. Instrum. Meth. B **291**, 29 (2012).
[21] Yu. Kudryavtsev, R. Ferrer, M. Huyse, P. Van den Bergh, and P. Van Duppen, Nucl. Instrum. Meth. B **297**, 7 (2013).
[22] S. Raeder et al., Nucl. Instrum. Meth. B **376**, 382 (2016).